



Co-published by  
**Institute of Fluid-Flow Machinery**  
Polish Academy of Sciences  
**Committee on Thermodynamics and Combustion**  
Polish Academy of Sciences

Copyright©2024 by the Authors under license CC BY 4.0

<http://www.imp.gda.pl/archives-of-thermodynamics/>



## Numerical assessment of solar air heater performance having a broken arc and broken S-shaped ribs as roughness

Shivam Haldia<sup>a</sup>, Vijay Singh Bisht<sup>a</sup>, Prabhakar Bhandari<sup>b\*</sup>, Lalit Ranakoti<sup>c</sup>, Akashdeep Negi<sup>c</sup>

<sup>a</sup>Department of Thermal Engineering, Faculty of Technology, Veer Madho Singh Bhandari Uttarakhand Technical University, Dehradun, Uttarakhand-248007, India

<sup>b</sup>Department of Mechanical Engineering, School of Engineering and Technology, K. R. Mangalam University, Gurgaon, Haryana-122103, India

<sup>c</sup>Department of Mechanical Engineering, Graphic Era Deemed to University, Clement Town, Dehradun, Uttarakhand-248002, India

\*Corresponding author email: prabhakar.bhandari40@gmail.com

Received: 23.11.2023; revised: 28.12.2023; accepted: 19.03.2024

### Abstract

This research article aims to provide a detailed numerical study of the multifaceted impact of S-shaped and broken arc roughness on solar air heaters. Therefore, a strong comparison was made between the modified heaters and smooth heaters for Reynolds numbers ranging from 2 000–22 000. Also, the impact of two parameters, i.e. pitch and gap was analyzed to optimize the performance of the heater. The gap varies from 0.3 mm to 0.9 mm in both types of ribs with a step size of 0.2 mm. Afterwards, the pitch distance between both types of roughness was varied from 15 mm to 25 mm in the step size of 5 mm. Notably, it has been observed that among all the considered configurations, the gap length of 0.9 mm and pitch length of 25 mm have shown significant improvements in heat transfer characteristics. The specific combination of the gap of 0.9 mm and pitch of 25 mm has demonstrated better heat transfer capabilities at the expense of an increased friction factor. Lastly, the thermal performance factor of the systems was analyzed and reported. It was reported that the pitch length of 25 mm and gap length of 0.9 mm have shown a maximum thermal performance factor value from 2.9 to 3.3, while the pitch length of 25 mm and gap length of 0.3 mm have depicted the lowest thermal performance factor value. In terms of the overall performance, i.e. the thermal performance factor, the combination with a gap of 0.9 mm and pitch of 25 mm has shown the best performance, while a gap of 0.3 mm and pitch of 25 mm has yielded the worst performance.

**Keywords:** Solar air heater; Thermal performance factor; S-shaped ribs; Broken arc; Numerical study

Vol. 45(2024), No. 1, 23–31; doi: 10.24425/ather.2024.150435

Cite this manuscript as: Haldia, S., Bisht, V.S., Bhandari P., Ranakoti, L., & Negi, A. (2024). Numerical assessment of solar air heater performance having a broken arc and broken S-shaped ribs as roughness. *Archives of Thermodynamics*, 45(1), 23–31.

### 1. Introduction

The combustion of conventional fuels, including coal, oil, and natural gases releases harmful gases with significant adverse effects on the environment. The limited availability of these conventional fuels has driven towards alternative sustainable and reliable sources, such as solar energy, wind energy, tidal energy, and more. Solar energy has emerged as a leading contender among these alternatives playing a pivotal role in reducing our dependency on conventional fuels by a substantial 40 % over the

past few decades [1]. Its application can be seen in various sectors e.g., heating and cooling industries, water desalination, generation of electricity, automobile industries and so on [2–4]. However, harnessing the potential of solar energy always remains a challenge. Adding to this literature, Jani [5] has suggested solar air heaters (SA-heaters) as the best medium for harnessing solar energy in the form of heat.

SA-heaters transfer thermal radiation from the sun to the working fluids i.e., air. However, SA-heaters deal with the inherent drawback of lower thermal efficiency due to the low

## Nomenclature

$C_p$  – specific heat, J/(kgK)  
 $f$  – friction factor  
 $G$  – gap length in broken arc and broken S-shaped ribs, mm  
 $k$  – thermal conductivity, W/(mK)  
 $Nu$  – average Nusselt number  
 $p$  – pressure, Pa  
 $P$  – pitch, mm  
 $Pr$  – Prandtl number  
 $Re$  – Reynolds number,  $Re = Dv\rho/\mu$   
 $T$  – temperature, K  
 $TPF$  – thermal performance factor  
 $t$  – time, s  
 $u, v, w$  – velocity components, m/s

$x, y, z$  – coordinates

## Greek symbols

$\alpha$  – thermal diffusivity,  $m^2/s$   
 $\mu$  – dynamic viscosity, Pa·s  
 $\rho$  – density,  $kg/m^3$

## Subscripts and Superscripts

$in$  – inlet  
 $r$  – roughened  
 $s$  – smooth

## Abbreviations and Acronyms

TPF – Thermal Performance Factor  
 SA-heater – Solar Air heater

thermal conductivity of air and reduce heat transfer from the absorber plate to the air. The airflow in SA-heaters is more often in a turbulent regime due to which thin laminar viscous sub-layers are formed near the absorber plate. Therefore, this laminar viscous sublayer can adversely affect the heat transfer rate [6]. To break the laminar viscous layer, various arrangements have been proposed on the absorber plate. Also, the similarity in the working of SA-heaters with various equipment like heat exchangers, car radiators, etc., is often considered by design researchers [7–9]. The use of artificial roughness like baffles, ribs, twisted tapes, dimples, etc., can mitigate the current associated problems [10–13].

A solar air heater with ribs of a square, rectangle, chamfered, circle, semi-circle, and triangle shape was investigated computationally by Chaube et al. [14]. The most effective thermo-hydraulic performance was reported for rectangular ribs. Additionally, it was observed that the data value is precisely predicted by the k- $\omega$  SST model, which is the shear stress transport turbulence model. Similarly, W-shaped ribs in upward and downward directions were analyzed by Lanjewar et al. [15]. It was observed that W-downward ribs have better thermo-hydraulic performance compared to W-upward ribs. Apart from this, multiple broken arcs and circular protrusions were used as roughness in a solar air heater in a novel way by Semalty et al. [16]. It was observed that multiple broken arcs and circular protrusions designs significantly enhance the solar air heater thermal performance with the least amount of frictional pressure drop. Furthermore, a numerical analysis was performed, by roughening the absorber plate with 45° Z-shaped baffles [17]. It was reported that a desirable blockage ratio of 0.3 produced optimum performance.

Different shape of tabulators has a significant impact on enhancing the performance of SA-heaters. Therefore, Ghildyal et al. [18] propose three different shaped turbulators i.e., D-shaped, reverse D-shaped and U-shaped for SA-heaters. It was observed that the U-shaped turbulator performs better in terms of overall performance compared to the other two configurations. Singh et al. [19] analyzed the effect of dimple roughness in S-shaped patterns in SA-heaters through computational work. For all arrangements, the dimple dimension of 2.8 mm and relative pitch roughness of 10 at the Reynold number (Re) of 20 000 resulted in the highest thermo hydraulic performance value of 2.15.

Apart from this, nanoparticles play a vital role in the thermal industry for obtaining better heat transfer rates [20]. However, due to their own advantages and disadvantages, hybrid nanofluids came into existence and may offer a tradeoff between them. For instance, Asghar et al. [21] performed a numerical study on the impact of hybrid nanofluid (Al<sub>2</sub>O<sub>3</sub>-Cu base) over vertical shrinking sheets using partial slip conditions. From this study, the enhancement in heat transfer was observed along with the rise in thermal slip and temperature distribution. Additionally, the influence of various parameters such as the concentration of nanoparticles, viscous dissipation, Biot number, thermal radiation and suction effect were investigated on shrinking surfaces. The study was performed using MATLAB tool using the bvp4c algorithm. During the study significant improvement in heat transfer was observed for hybrid nanofluid, compared to base fluids [22]. Moreover, the paper [23] investigated radiative 2D flow over a horizontal surface. The combined effect of magnetic, suction and velocity slip conditions was analyzed with hybrid nanofluids. The Eckert number was found to be an influential parameter to study. It has been observed that with the rise in the Eckert number, the increased temperature of the hybrid nanofluid resulted in a higher heat transfer rate [24–27].

Based on the literature study, turbulator shapes and hybrid nanofluids can significantly affect the thermo-hydraulic performance of SA-heaters. However, using hybrid nanofluids as a working fluid increases the operating cost of the system. Therefore, introducing roughness on the absorber plate is the most prominent and economical method to trade between cost and performance. However, according to the best knowledge of the authors, S-shaped and broken arc roughness configurations have not been reported as far in the SA-heaters. These configurations are integrated with the smooth absorber plate to disturb the viscous sublayer. Furthermore, a numerical investigation was carried out to analyze the effect of variation in Re number on the fluid flow characteristics, heat transfer, and friction. The present numerical work may show several limitations. Firstly, the existing literature may lack comprehensive studies on the combined impact of broken arc and broken S-shaped ribs, leaving a gap in understanding their synergistic effects on heat transfer and fluid dynamics. Additionally, the numerical models used in these assessments might oversimplify the real-world conditions, neglecting factors such as thermal radiation, material

properties, and ambient conditions. Furthermore, the majority of studies may focus on specific geometric configurations, and a lack of generalization across various parameters could limit the applicability of the findings. The experimental validation of numerical simulations is crucial for the reliability of results, but this aspect may be inadequately addressed in the available research. Overall, there is a need for more comprehensive investigations that consider a broader range of parameters and incorporate experimental validation to enhance the accuracy and applicability of numerical assessments in the context of solar air heater performance with broken arc and broken S-shaped ribs.

## 2. Numerical methodology

In this section, the numerical methodology carried out for the present study of the SA-heater has been presented. The rectangular air duct design was selected and modified with the broken S and broken arc-shaped ribs with different gaps and pitches. Modified SA-heaters were simulated and later compared with the conventional design model having a smooth absorber. The

performance was evaluated by computing different parameters i.e., the average Nusselt number ( $Nu$ ) and friction factor.

### 2.1. Geometrical modelling of modified SAH

The solar air heater considered for this study has a rectangular cross-section with dimensions  $300 \times 25$  mm as the width and height. The length of the SA-heater was 2400 mm. Further, the roughness of S-shaped and broken arc configurations was introduced in the form of ribs over the smooth absorber surface. The hydraulic diameter ( $D_h$ ) of the present shape is 46.154 mm. Furthermore, Fig. 1 represents the geometrical construction of an SA-heater with a detailed view of the roughness. The total length of the solar air heater was categorized into three zones i.e., (1) entrance section of length 525 mm, (2) roughness section of length 1000 mm, and (3) exit section of length 875 mm. The diagram of the complete SA-heater is shown in Fig. 1. The entrance length is provided to develop the flow for the roughness zone.

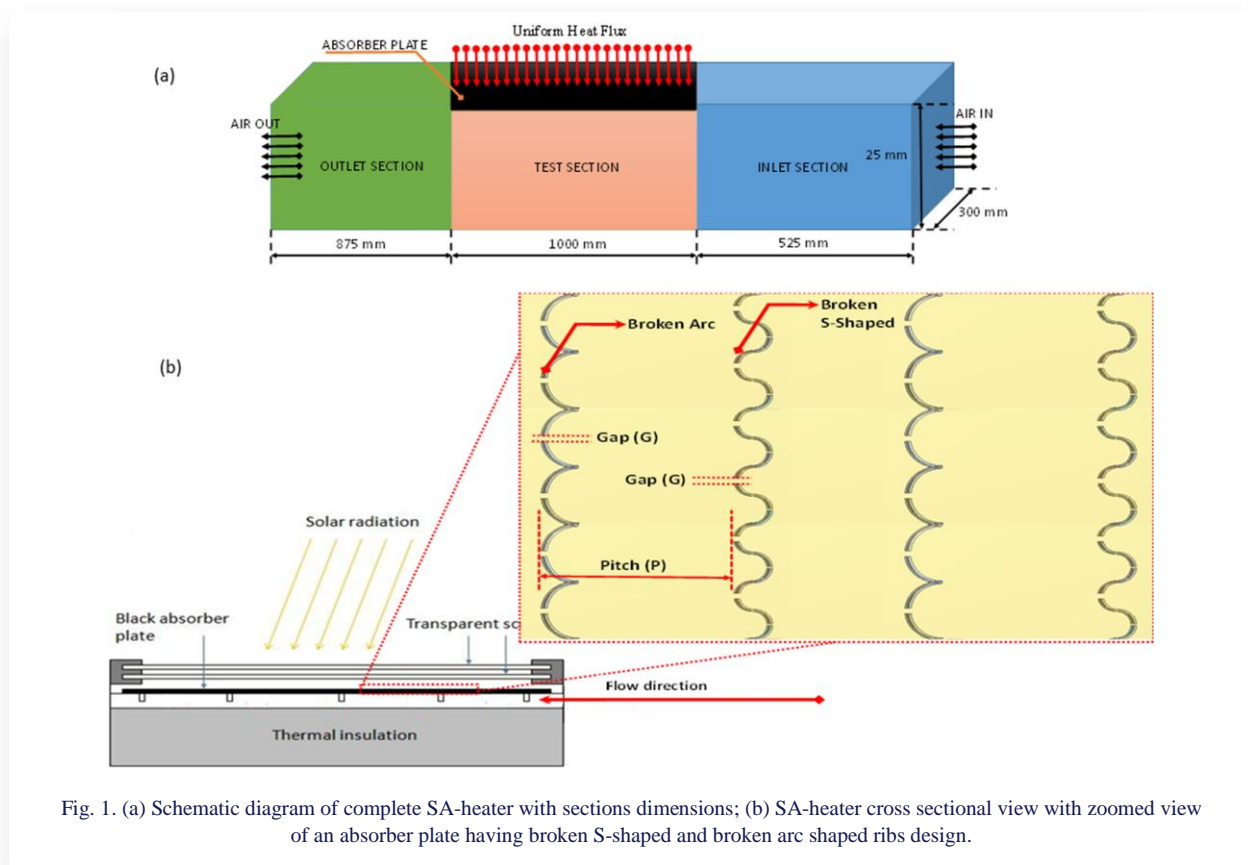


Fig. 1. (a) Schematic diagram of complete SA-heater with sections dimensions; (b) SA-heater cross sectional view with zoomed view of an absorber plate having broken S-shaped and broken arc shaped ribs design.

The roughness of height 1.4 mm was used for different sets of configurations of the SA-heater. In the present work, two different geometrical parameters (gap and pitch) have been varied simultaneously. Firstly, the gap width in the broken arc and broken S-shaped ribs was inserted over the smooth absorber plate. The gap ( $G$ ) varies from 0.3 mm to 0.9 mm for both rib configurations with a step size of 0.2 mm. Secondly, the pitch distance between both configurations of rib roughness varied from 15 mm to 25 mm with a step size of 5 mm. These parameters were

opted for the creation of more reattachment zones in the fluid flow with the roughened surface.

### 2.2. Governing equations and assumptions

Three important laws, i.e. the conservation of mass (continuity), momentum (N-S) and energy equations are used to govern the problems related to flow. They are expressed by Eqs. (1–5), respectively:

a) **Continuity equation.** The continuity equation is the mathematical statement of the concept of conservation of mass applied to an elemental control volume within a fluid in motion, and it is evaluated by using Eq. (1) [18–19]:

$$\frac{\partial \bar{u}}{\partial x} + \frac{\partial \bar{v}}{\partial y} + \frac{\partial \bar{w}}{\partial z} = 0. \quad (1)$$

This is the mass continuity equation for three-dimensional steady flow.

b) **Momentum equation.** It can be calculated by using Eqs. (2–4) [18–19]:

x–momentum equation:

$$\left( \bar{u} \frac{\partial \bar{u}}{\partial x} + \bar{v} \frac{\partial \bar{u}}{\partial y} + \bar{w} \frac{\partial \bar{u}}{\partial z} \right) = -\frac{1}{\rho} \frac{\partial p}{\partial x} + \nu \left( \frac{\partial^2 \bar{u}}{\partial x^2} + \frac{\partial^2 \bar{u}}{\partial y^2} + \frac{\partial^2 \bar{u}}{\partial z^2} \right), \quad (2)$$

y–momentum equation:

$$\left( \bar{u} \frac{\partial \bar{v}}{\partial x} + \bar{v} \frac{\partial \bar{v}}{\partial y} + \bar{w} \frac{\partial \bar{v}}{\partial z} \right) = -\frac{1}{\rho} \frac{\partial p}{\partial y} + \nu \left( \frac{\partial^2 \bar{v}}{\partial x^2} + \frac{\partial^2 \bar{v}}{\partial y^2} + \frac{\partial^2 \bar{v}}{\partial z^2} \right), \quad (3)$$

z–momentum equation:

$$\left( \bar{u} \frac{\partial \bar{w}}{\partial x} + \bar{v} \frac{\partial \bar{w}}{\partial y} + \bar{w} \frac{\partial \bar{w}}{\partial z} \right) = -\frac{1}{\rho} \frac{\partial p}{\partial z} + \nu \left( \frac{\partial^2 \bar{w}}{\partial x^2} + \frac{\partial^2 \bar{w}}{\partial y^2} + \frac{\partial^2 \bar{w}}{\partial z^2} \right). \quad (4)$$

c) **Energy equation.** If the flow is continuous and incompressible with constant thermal conductivity, there is no compression effect and no heat generation. In this case, no viscous heating is generated and the following equation can be used [18–19, 28]:

$$u \frac{\partial T}{\partial x} + v \frac{\partial T}{\partial y} + w \frac{\partial T}{\partial z} = \alpha \left( \frac{\partial^2 T}{\partial x^2} + \frac{\partial^2 T}{\partial y^2} + \frac{\partial^2 T}{\partial z^2} \right). \quad (5)$$

The turbulence model is the typical  $k-\epsilon$  model. It is the most frequent turbulence model applied in solar air heater applications. The following assumptions were taken into account during numerical simulations of the solar air heater models to simplify the numerical procedure:

- (1) The flow must be steady i.e.,  $\frac{\partial \rho}{\partial t} = 0$ .
- (2) Variation of the pressure in y direction is zero i.e.,  $\frac{\partial p}{\partial y} = 0$ .
- (3) The shear force in y direction is zero i.e.,  $\frac{\partial \tau}{\partial y} = 0$ .
- (4) The body force due to gravity is neglected.
- (5) The flow must be incompressible i.e.,  $\frac{\partial \rho}{\partial x}, \frac{\partial \rho}{\partial y}, \frac{\partial \rho}{\partial z} = 0$ .
- (6) The flow must be fully developed, while approaching the test section.
- (7) The axial heat conduction in the fluid is negligible.
- (8) The properties of the air must be constant.

### 2.3. Boundary conditions and material properties

During the numerical modelling for the study, a constant heat flux ( $q$ ) of 1200 W/m<sup>2</sup> is applied on the absorber plate. Additionally, the Re number of working fluid, i.e. air is varied from 2 000 – 22 000 with the step size of 4 000. The flow is considered turbulent, having the turbulent kinetic energy intensity of 5%. The temperature of the inlet air ( $T_{in}$ ) flowing inside the SA-heater channels is 300 K. Aluminium is used as substrate material for the SA-heater. It has great machinability, high thermal

conductivity; it is easily available, and economical compared to other materials such as stainless steel (SS). Table 1, tabulates the thermo-physical properties of aluminium and air considered for simulations. It was observed that the variation of properties with respect to temperature is very minimal. So, constant properties were considered during the simulation.

Table 1. Thermo-physical properties categorization of the aluminum and air [19].

Properties	Symbol	Unit	Aluminium	Air
Density	$\rho$	kg/m <sup>3</sup>	2719	1.225
Specific heat	$C_p$	J/(kgK)	871	1006.4
Thermal conductivity	$k$	W/(mK)	202.4	0.707
Viscosity	$\mu$	Pa s	---	1.7894e-05

### 2.4. Mesh generation and grid independence test

Firstly, the geometry was designed, and the model was discretized using different methods. The smooth solar air heater duct does not create much obstruction in mesh generation due to its simplicity and symmetry. In the presence of ribs of different shape, it is necessary to understand flow physics near the roughness. So, fine meshing was created in the vicinity of rib roughness as depicted in Fig. 2.

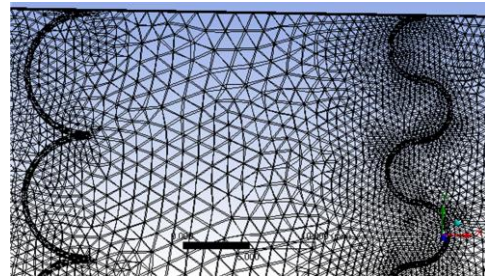


Fig. 2. Meshing of the absorber plate near the ribs.

Using an unstructured grid, the geometry was discretized and an adaptive refinement method was used. When the adaption is employed appropriately, the resulting mesh is most favourable for the flow solution. Further, a grid independence test was performed on the roughened solar air heater to see the influence of grid size. Table 2 highlights the variation of the average Nu number with the number of elements.

Table 2. Grid independence test on the roughened solar air heater.

No. of elements	Average Nu number	% variation
65 932	110.668	14%
130 832	95.170	51.65%
845 671	46.014	2.0%
912 839	46.964	--

It was observed that increasing the cell number beyond 845 671 elements, the variation observed is less than 5%. There-

fore, to avoid waste of the computational resources, the grid of 845 671 elements was proposed for the study.

## 2.5. Validation of the numerical model

The numerical model was validated by comparing the results with those of the smooth solar air heater. The obtained results were compared with those found from two well-known Eqs. (6) and (7). Firstly, the average Nu number from the present work was compared with that obtained from the Dittus-Boelter equation as in Eq. (6) [29]:

$$Nu = 0.023 \times Re^{0.8} \times Pr^{0.4}, \quad (6)$$

where Re is the Reynolds number and Pr is the Prandtl number. The results are plotted for Re ranging from 2 000–22 000 as presented in Fig. 3. A slight variation of 3–5% is observed between the compared models. Furthermore, another parameter, that is the friction factor  $f$  was calculated and compared with that of the smooth SA-heater found from the Blasius friction equation as in Eq. (7) [29]:

$$f = 0.0791Re^{-0.25}. \quad (7)$$

The obtained results for the friction factor are also found to be in good agreement, which validates our numerical model.

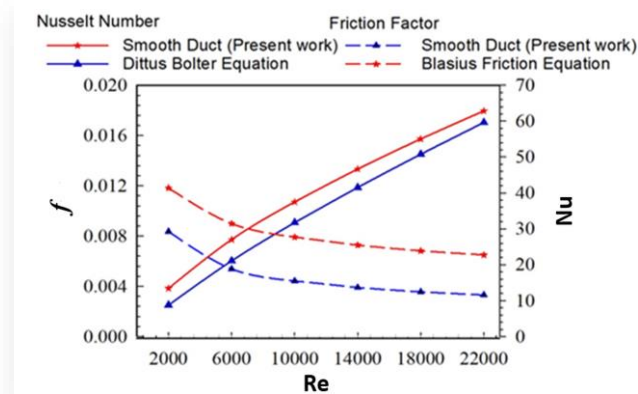


Fig. 3. Validation of the present numerical model of smooth duct based on the previously known empirical correlations.

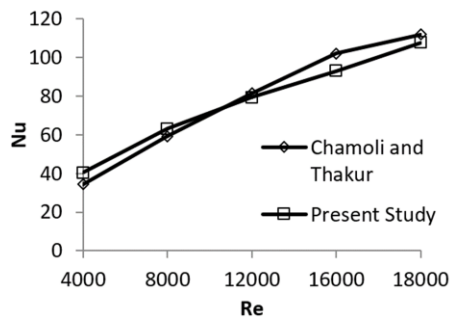


Fig. 4. Validation of present methodology with previous experimental work of Chamoli and Thakur [30].

The validity of the computational model is also established through a rigorous comparison of the Nu number outcomes generated by the current methodology with those obtained through

experimental investigations conducted by Chamoli and Thakur [30], as illustrated in Fig. 4. To achieve this, a geometric configuration akin to that employed by Chamoli and Thakur [30] has been replicated and subjected to simulation under identical operating conditions. The assessment reveals an average absolute deviation of 7.86% between the computational and experimental data for the Nu number, affirming the reliability of the computational approach.

## 3. Results and discussion

The outcome of introducing roughness (broken arc ribs and broken S-shaped ribs) to the absorber surface of the SA-heater is presented in this section. The outcomes of the roughened SA-heaters for variable constructional parameters are presented and compared with smooth SA-heaters. Introducing roughness in SA-heaters stimulates enhanced heat transfer processes with an increase in friction factor coefficient [30]. The influence of varying gaps and pitches on thermal hydraulic performance is evaluated and presented. Additionally, the Re number was varied between 2 000–22 000.

### 3.1. Effect of geometrical variation on heat transfer characteristics

The Nusselt number is an important parameter for evaluating the heat transfer capabilities of different SA-heater configurations. Figure 5, represents the variation of the average Nu number with the Re number for different SA-heater configurations. The  $x$ -axis represents the variation of Re while  $y$ -axis represents the Nu number. During the study, the gap was varied from 0.3 mm to 0.9 mm in Figs. 4 to 5, while the pitch was kept constant for all the cases, i.e. 15–25 mm.

At  $G = 0.3$  mm, it is observed that the Nu number increases along with the increase in pitch from 15 mm to 20 mm; further increase of the pitch value decreases the Nu value, irrespective of the Re number. The best performance was reported at the pitch length of 20 mm. The difference in the Nu number for the configurations  $P = 15$  mm and  $P = 25$  mm is very minimal, while a reasonable amount of increment was observed in the  $P = 20$  mm configuration for all Re values. It is interesting to note that the pattern for different pitch lengths changes with an increase in gap length. The earlier pitch of 20 mm has yielded a better performance while for the gap length varying from 0.5 mm to 0.9 mm, the pitch of 25 mm has shown better heat transfer capabilities. Also, the gap between the  $P = 20$  mm and  $P = 25$  mm kept on increasing from  $G = 0.5$  mm to  $G = 0.9$  mm as visualized in Fig. 4 (b–d). Among all the configurations considered, the gap length of 0.9 mm and pitch length of 25 mm has shown the best performance.

### 3.2. Effect of geometrical variation on hydraulic performance

The pressure drop and friction factor are important parameters to be evaluated for the hydraulic performance of SA-heater configurations. In the present work, the friction factor was computed for all configurations. The influence of geometrical parameters and operating parameters on friction factor was depicted

ted in Fig. 6. It is observed that the pitch length of 25 mm has shown the largest value of friction factor, irrespective of gap length and Re number. Further, there is a minimal difference in friction factor observed between  $P = 20$  mm and  $P = 25$  mm, due to very little change in fluid flow characteristics. Also, there appears a significant increase in friction factor for a change in

pitch length configuration from 15 mm to 20 mm. Further, the lowest friction factor was observed for the smooth solar air heater duct, which is due to no disturbance in fluid flow across the length of the solar air heater. A sudden drop was observed in all configurations when the Re number changed from 2 000 to 6 000 due to the change in fluid flow from laminar to turbulent.

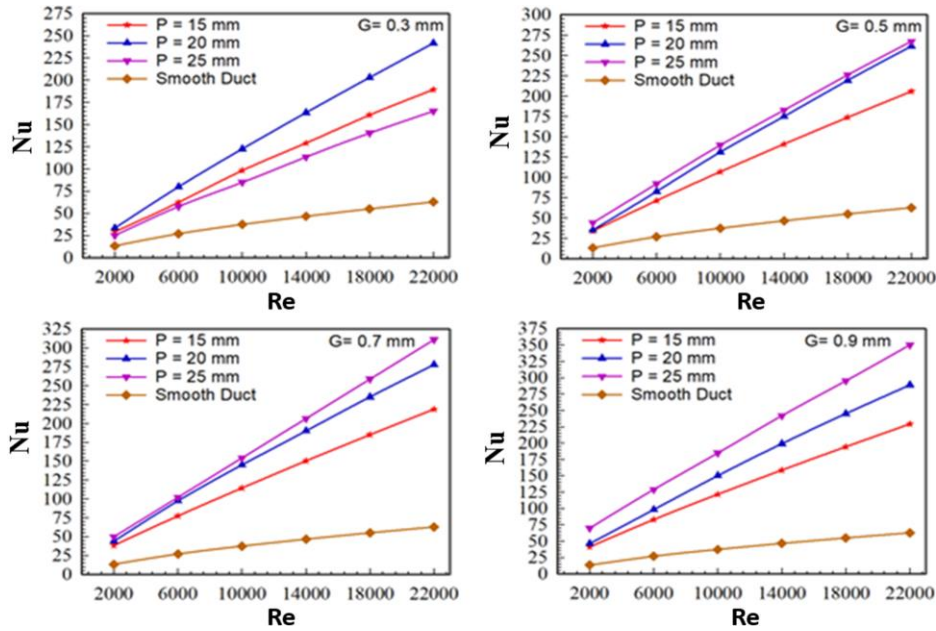


Fig. 5. Effects of varying gap and Re number on Nu number for modified SA-heaters (for  $G = 0.3$  mm,  $0.5$  mm,  $0.7$  mm and  $0.9$  mm).

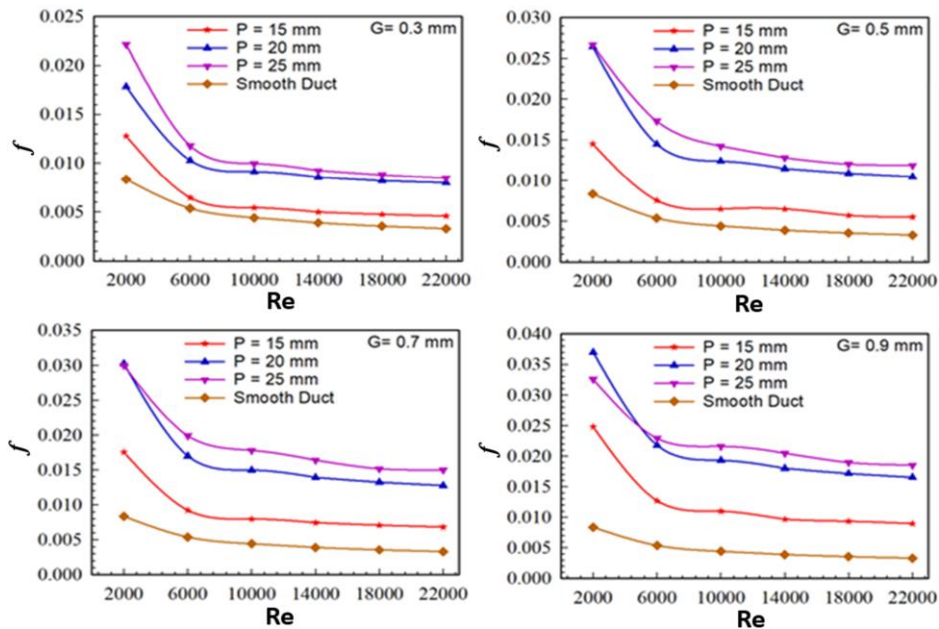


Fig. 6. Variation of  $f$  for varying Re number for modified solar air heaters (for  $G = 0.3$  mm,  $0.5$  mm,  $0.7$  mm and  $0.9$  mm).

### 3.3. Effects of geometrical variations on fluid flow characteristics

The velocity contours were plotted for a constant value of Re number for different configurations. Figure 7 shows velocity contours of SA-heaters for the pitch length of 25 mm having the

gap length varying from 0.3 mm to 0.9 mm for the Re number of 22 000. It was observed that for  $G = 0.3$  mm, there is a very large reattachment zone formed around the surface. This reattachment zone kept on decreasing with the increase in gap length. Among all the configurations, that of  $G = 0.9$  mm and  $P = 25$  mm has shown the most favourable fluid flow conditions.

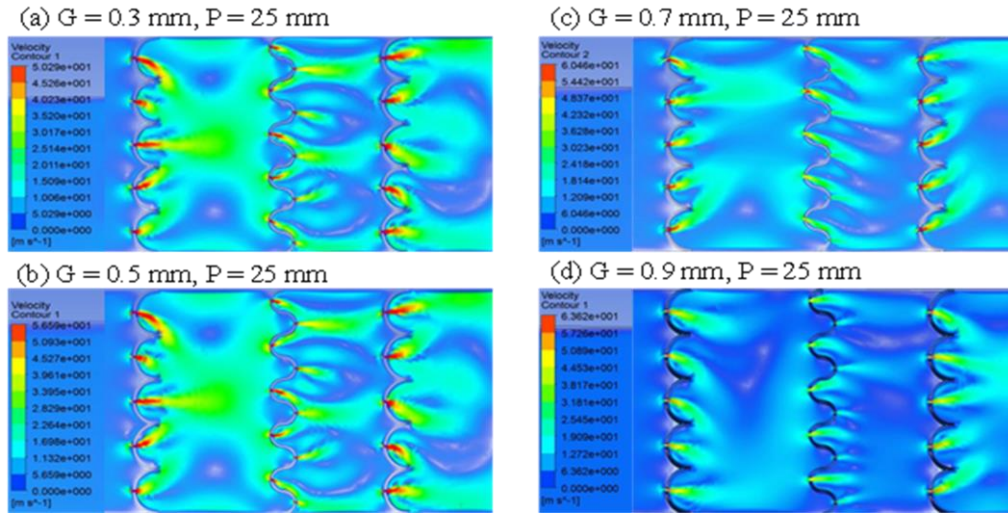


Fig. 7. Velocity contours for different configurations of roughened SA-heater: (a)  $G = 0.3$  mm,  $P = 25$  mm; (b)  $G = 0.5$  mm,  $P = 25$  mm; (c)  $G = 0.7$  mm,  $P = 25$  mm; (d)  $G = 0.9$  mm,  $P = 25$  mm.

### 3.4. Thermo-hydraulic performance

As mentioned, the integration of roughness over the absorber plate in the SA-heaters improves heat transfer capabilities of the SA-heaters. Also, increased values of pressure drop can be observed corresponding to the heat transfer improvement. To identify whether the roughness used yields better heat transfer capability than pressure drop losses, there are various parameters to measure the thermo-hydraulic performance, like the coefficient of performance, thermal performance factor (TPF), efficiency, etc. [32–35]. Figure 8 represents the variation of TPF with Re for the used SA-heater configurations.

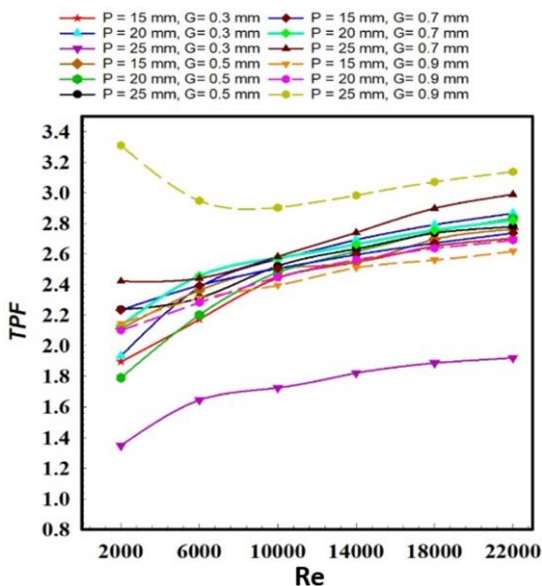


Fig. 8. Variation of thermal performance factor with Reynolds number for roughened SA-heater configurations.

In the present work, TPF is opted to evaluate the design efficiency. TPF was evaluated using Eq. (8). TPF is used often in

the literature as it helps researchers comprehend the overall performance of thermal devices

$$TPF = \frac{(Nu_r/Nu_s)}{(f_r/f_s)^{1/3}} \quad (8)$$

It was observed that the pitch length of 25 mm and gap length of 0.9 mm has shown a maximum TPF value from 2.9 to 3.3, while the pitch length of 25 mm and gap length of 0.3 mm has depicted the lowest TPF value, irrespective of the Re number. All other configurations have TPF values ranging between them.

### 4. Conclusions and scope of future work

In the present article, a numerical study was conducted on the SA-heater modified with ribs of broken S-shape and broken arc shape. Through this research, authors have demonstrated the potential of these specific roughness configurations to enhance heat transfer and improve the overall efficiency of solar air heaters. This work contributes to the advancement of sustainable energy technologies, offering practical solutions that can be implemented to harness solar energy more efficiently in various applications, such as space heating, water heating and industrial processes. The study was performed using the ANSYS Fluent software. During the study, three important parameters (Re number, gap, and pitch) were varied to obtain the best optimum value of each for the improved heat transfer rate. The Re number was varied from 2 000–22 000, while the pitch was varied from 15–25 mm and the gap length was varied from 0.3–0.9 mm. For this study, a constant heat flux of 1 200 W/m<sup>2</sup> was provided to the system. Various contributing parameters such as the Nu number, friction factor and thermal performance factor were evaluated and validated with the smooth surface absorber based SA-heater. On the basis of the study, a few conclusions were made as follows:

1. Among all the configurations considered, the gap length of 0.9 mm and pitch length of 25 mm has shown the best performance and a significant improvement in the Nu number.

2. The pressure drop and friction are important parameters to be evaluated for the hydraulic performance of SA-heater configurations
3. Minimal variations in friction factor were observed between  $P = 20$  mm and  $P = 25$  mm due to very little change in fluid flow characteristics. However, a sudden pressure drop was observed in all configurations when Re changed from 2 000 to 6 000 due to the change in fluid flow from laminar to turbulent.
4. It was observed that the pitch length of 25 mm and gap length of 0.9 mm have shown the maximum thermal performance factor value from 2.9 to 3.3, while the pitch length of 25 mm and gap length of 0.3 mm have depicted the lowest thermal performance factor value.
5. These modifications can be experimentally integrated with the SA-heater device to improve the overall performance of the system.

## References

- [1] Habib, K., & Wenzel, H. (2014). Exploring rare earths supply constraints for the emerging clean energy technologies and the role of recycling. *Journal of Cleaner Production*, 84, 348–359. doi: 10.1016/j.jclepro.2014.04.035
- [2] Kumar, A., Bhandari, P., & Rawat, K. (2021). Numerical Simulation of Solar Air Heater using Paraffin Wax-Aluminum Compound as Phase Changing Material. *Aptisi Transactions on Technopreneurship*, 3(2), 164–170. doi: 10.34306/att.v3i2.199
- [3] Varshney, L., Bhandari, P., & Bisht, V.S. (2014). Performance Evaluation of Hybrid Solar Water Heating System Using Wire Screen Packed Solar Air Heater. *International Journal of Engineering Research and Application*, 311–316.
- [4] Bhandari, P., Varshney, L., & Bisht, V.S. (2018). Numerical analysis of hybrid solar water heating system using wire screen packed solar air heater. *1st International Conference on New Frontiers in Engineering, Science and Technology*, 1, 415–422, 8–12 January, New Delhi, India.
- [5] Jani, D.K.S. (2023). Design and performance analysis of a solar air (SA) heater with phase change material (PCM) heat storage for residential applications. *International Journal of Innovative Research in Engineering and Management*, 10(4), 106–113. doi: 10.55524/ijirem.2023.10.4.13
- [6] Bisht, A.S., Bisht, V.S., Bhandari, P., Rawat, K.S., Alam, T., & Blecich, P. (2023). The use of a vortex generator for the efficient cooling of lithium-ion batteries in hybrid electric vehicles. *Processes*, 11, 500. doi: 10.3390/pr11020500
- [7] Thapa, R.K., Bisht, V.S., Rawat, K.S., & Bhandari, P. (2022). Computational analysis of automobile radiator roughened with rib roughness. *Journal of Heat and Mass Transfer Research*, 9(2), 209–218. doi: 10.22075/jhmtr.2023.27617.1382
- [8] Bhandari, P., Singh, J., Kumar, K., & Ranakoti, L. (2022). A review on active techniques in microchannel heat sink for miniaturisation problem in electronic industry. *Acta Innovations*, 45, 45–54. doi: 10.32933/ActaInnovations.45.4
- [9] Singh, B.P., Bisht, V.S., Bhandari, P., & Rawat, K.S. (2021). Thermo-fluidic modelling of a heat exchanger tube with conical shaped insert having protrusion and dimple roughness. *Aptisi Transactions on Technopreneurship*, 3(2), 13–29. doi: 10.34306/att.v3i2.200
- [10] Thapa, R.K., Bisht, V.S., Bhandari, P., & Rawat, K.S. (2022). Numerical study of car radiator using dimple roughness and nanofluid. *Archives of Thermodynamics*, 43(3), 125–140. doi: 10.24425/ather.2022.143175
- [11] Singh, B.P., Bisht, V.S., & Bhandari, P. (2021). Numerical Study of Heat Exchanger Having Protrusion and Dimple Roughened Conical Ring Inserts. In *Advances in Fluid and Thermal Engineering* (pp. 151–161). Springer Singapore. doi: 10.1007/978-981-16-0159-0\_14
- [12] Bisht, V.S., Patil, A.K., & Gupta, A. (2018). Review and performance evaluation of roughened solar air heaters. *Renewable and Sustainable Energy Reviews*, 81, 954–977. doi: 10.1016/j.rser.2017.08.036
- [13] Alam, T., & Kim, M.H. (2016). Numerical study on thermal hydraulic performance improvement in solar air heater duct with semi ellipse shaped obstacles. *Energy*, 112, 588–598. doi: 10.1016/j.energy.2016.06.105
- [14] Chaube, A., Sahoo, P.K., & Solanki, S.C. (2006). Effect of roughness shape on heat transfer and flow friction characteristics of solar air heater with roughened absorber plate. *WIT Transactions on Engineering Sciences*, 53, 43–51. doi: 10.2495/HT060051
- [15] Lanjewar, A., Bhargoria, J.L., & Sarviya, R.M. (2011). Experimental study of augmented heat transfer and friction in solar air heater with different orientations of W-rib roughness. *Experimental thermal and fluid science*, 35, 986–995. doi: 10.1016/j.expthermflusci.2011.01.019
- [16] Semalty, A., Bisht, V.S., Bhandari, P., Rawat, K., Singh, J., Kumar, K., & Dixit, A.K. (2022). Thermodynamic investigation on solar air heater having roughness as multiple broken arc and circular protrusion. *Materials Today: Proceedings*, 69(2), 181–186. doi: 10.1016/j.matpr.2022.08.336
- [17] Bohra, J., Bisht, V.S., Bhandari, P., Rawat, K.S., Singh, J., Kumar, K., & Rawat, B. (2022). Effect of variable blockage height ratio on performance for solar air heater roughened with 45° Z-shaped baffles. *Materials Today: Proceedings*, 69(2), 153–157. doi: 10.1016/j.matpr.2022.08.279
- [18] Ghildyal, A., Bisht V.S., Bhandari, P., & Rawat K.S. (2023). Effect of D-shaped, reverse D-shaped and U-shaped turbulators in solar air heater on thermo-hydraulic performance. *Archives of Thermodynamics*, 44(2), 3–20. doi: 10.24425/ather.2023.146556
- [19] Singh, J., Bisht, V.S., Bhandari, P., Kumar, K., Singh, J., Alam, T., Dixit, S., Singh, S., & Khusnutdinov, R. (2023). Computational parametric investigation of solar air heater with dimple roughness in S-shaped pattern. *International Journal on Interactive Design and Manufacturing (IJIDeM)*. doi: 10.1007/s12008-023-01392-8
- [20] Asghar, A., Lund, L.A., Shah, Z., Vrinceanu, N., Deebani, W., & Shutaywi, M. (2022). Effect of thermal radiation on three-dimensional magnetized rotating flow of a hybrid nanofluid. *Nano-materials*, 12(9), 1566. doi: 10.3390/nano12091566
- [21] Asghar, A., Ying, T.Y., & Zaimi, K. (2022). Two-dimensional mixed convection and radiative  $Al_2O_3$ -Cu/ $H_2O$  hybrid nanofluid flow over a vertical exponentially shrinking sheet with partial slip conditions. *CFD Letters*, 14(3), 22–38. doi: 10.37934/cfdl.14.3.2238
- [22] Asghar, A., Vrinceanu, N., Ying, T.Y., Lund, L.A., Shah, Z., & Tirth, V. (2023). Dual solutions of convective rotating flow of three-dimensional hybrid nanofluid across the linear stretching/shrinking sheet. *Alexandria Engineering Journal*, 75(3), 297–312. doi: 10.1016/j.aej.2023.05.089
- [23] Rasool, G., Xinhua, W., Lund, L.A., Yashkun, U., Wakif, A., & Asghar, A. (2023). Dual solutions of unsteady flow of copper-alumina/water based hybrid nanofluid with acute magnetic force and slip condition. *Heliyon*, 9, 22737. doi: 10.1016/j.heliyon.2023.e22737

- [24] Teh, Y. Y., & Ashgar, A. (2021). Three dimensional MHD hybrid nanofluid Flow with rotating stretching/shrinking sheet and Joule heating. *CFD Letters*, 13(8), 1–19. doi: 10.37934/cfdl.13.8.119
- [25] Lund, L. A., Asghar, A., Rasool, G., & Yashkun, U. (2023). Magnetized casson SA-hybrid nanofluid flow over a permeable moving surface with thermal radiation and Joule heating effect. *Case Studies in Thermal Engineering*, 50, 103510. doi: 10.1016/j.csite.2023.103510
- [26] Asghar, A., Chandio, A.F., Shah, Z., Vrinceanu, N., Deebani, W., Shutaywi, M., & Lund, L.A. (2023). Magnetized mixed convection hybrid nanofluid with effect of heat generation/absorption and velocity slip condition. *Heliyon*, 9(2), 13189. doi: 10.1016/j.heliyon.2023.e13189
- [27] Asghar, A., Ying, T.Y., & Zaimi, K. (2022), Two-dimensional magnetized mixed convection hybrid nanofluid over a vertical exponentially shrinking sheet by thermal radiation, joule heating, velocity and thermal slip conditions. *Journal of Advanced Research in Fluid Mechanics and Thermal Sciences*, 95(2), 159–179. doi: 10.37934/arfmts.95.2.159179
- [28] Saxena, A., & El-Sebaai, A.A. (2015). A thermodynamic review of solar air heaters. *Renewable and Sustainable Energy Reviews*, 43, 863–890. doi: 10.1016/j.rser.2014.11.059
- [29] Kumar, S., & Verma, S.K. (2020). Three-dimensional simulation and experimental validation of solar air heater having sinusoidal rib. *Energy Sources, Part A: Recovery, Utilization, and Environmental Effects*, 1–19. doi: 10.1080/15567036.2020.1818007
- [30] Chamoli, S., & Thakur, N.S. (2016) Correlations for solar air heater duct with V-shaped perforated baffles as roughness elements on absorber plate. *International Journal of Sustainable Energy*, 35(1), 1–20. doi: 10.1080/14786451.2013.857318
- [31] Alam, T., & Kim, M.K. (2017). Heat transfer enhancement in solar air heater duct with conical protrusion roughness ribs. *Applied Thermal Engineering*, 126, 458–469. doi: 10.1016/j.appltherm-eng.2017.07.181
- [32] Bhandari, P., Rawat, K.S., Prajapati, Y.K., Padalia, D., Ranakoti, L., & Singh, T. (2024). A review on design alteration in micro-channel heat sink for augmented thermohydraulic performance. *Ain Shams Engineering Journal*, 15(2), 102417. doi: 10.1016/j.asej.2023.102417
- [33] Bhandari, P., Padalia, D., Ranakoti, L., Khargotra, R., Andrés, K., & Singh, T. (2023). Thermo-hydraulic investigation of open micro prism pin fin heat sink having varying prism sides. *Alexandria Engineering Journal*, 69, 457–468. doi: 10.1016/j.aej.2023.02.016
- [34] Bhandari, P. (2022). Numerical investigations on the effect of multi-dimensional stepness in open micro pin fin heat sink using single phase liquid fluid flow. *International Communications in Heat and Mass Transfer*, 138, 106392. doi: 10.1016/j.icheatmasstransfer.2022.106392
- [35] Bhandari, P., Prajapati, Y.K., & Uniyal, A. (2022). Influence of three dimensionality effects on thermal hydraulic performance for stepped micro pin fin heat sink. *Meccanica*, 58(11), 2113–2129. doi: 10.1007/s11012-022-01534-4